Tandem Tilt-Wing Control Design Based on Sensory Nonlinear Dynamic Inversion

Daniel Milz and Marc May and Gertjan Looye

Tandem tilt-wing eVTOL aircraft have become increasingly popular in the last decade due to their advantages of efficient wing-borne cruise flight and reduced reliance on ground- based infrastructure. However, this comes at the cost of a complex flight control task, which entails the handling of the different flight regimes and the transition between them. Dynamic inversion-based control methods, especially sensory nonlinear dynamic inversion (sensory NDI), have shown promise in addressing this challenge. This paper presents the design and implementation of a sensory NDI-based angular rate and velocity inversion integrated with an optimization-based control allocation scheme, which is cascaded with a parallel attitude and flight path controller. The parallel control loops are designed to facilitate a full transition while utilizing all available degrees of freedom and control effectors. This control law is demonstrated on a strip theory-based 6-DoF flight dynamic model of a tandem tilt-wing configuration. The results indicate that the control law can effectively invert the dynamics within a subset of the flight envelope. In fact, decoupling the pitch angle from the flight path and the outbound transition maneuver works smoothly, whereas maneuvering into the post-stall regime leads to instabilities and needs to be addressed in future work.

Milz, Daniel and May, Marc and Looye, Gertjan (2024) Tandem Tilt-Wing Control Design Based on Sensory Nonlinear Dynamic Inversion. In: AIAA AVIATION FORUM AND ASCEND 2024, 2024. AIAA AVIATION FORUM AND ASCEND 2024, 29 Jul-02 Aug 2024, Las Vegas, NV. DOI: 10.2514/6.2024-4418

Tandem Tilt-Wing Control Design based on Sensory Nonlinear Dynamic Inversion

Daniel Milz* and Marc May† and Gertjan Looye‡
Institute of System Dynamics and Control, German Aerospace Center (DLR), 82234 Weßling, Germany

Tandem tilt-wing eVTOL aircraft have become increasingly popular in the last decade due to their advantages of efficient wing-borne cruise flight and reduced reliance on ground-based infrastructure. However, this comes at the cost of a complex flight control task, which entails the handling of the different flight regimes and the transition between them. Dynamic inversion-based control methods, especially sensory nonlinear dynamic inversion (sensory NDI), have shown promise in addressing this challenge. This paper presents the design and implementation of a sensory NDI-based angular rate and velocity inversion integrated with an optimization-based control allocation scheme, which is cascaded with a parallel attitude and flight path controller. The parallel control loops are designed to facilitate a full transition while utilizing all available degrees of freedom and control effectors. This control law is demonstrated on a strip theory-based 6-DoF flight dynamic model of a tandem tilt-wing configuration. The results indicate that the control law can effectively invert the dynamics within a subset of the flight envelope. In fact, decoupling the pitch angle from the flight path and the outbound transition maneuver works smoothly, whereas maneuvering into the post-stall regime leads to instabilities and needs to be addressed in future work.

I. Introduction

Transformational or transition vertical take-off and landing (VTOL) aircraft have become pivotal in the context of Advanced Air Mobility (AAM). They offer unparalleled flexibility to operate in confined spaces and enable novel operational concepts by seamlessly transitioning between hover and forward flight. Among the promising configurations are tandem tilt-wing electric VTOLs (eVTOLs), which combine the capability for vertical take-off and landings with an efficient cruise flight, all while using a single propulsion system for all flight phases [1]. However, transformational VTOLs, especially tandem tilt-wings, have intricate mechanics at the tilting mechanism and exhibit complex aerodynamic characteristics, necessitating novel modeling approaches to accurately capture propeller-wing and wing-wing interactions [2, 3]. Moreover, the transition between different flight phases represents a complex and little-studied phenomenon that must be handled in order to allow tilt-wing operations [4]. Nevertheless, multiple endeavors have been conducted on (tandem) tilt-wing configurations, including the CL-84 [5], Airbus A^3 Vahana [6], NASA LA-8 [7], and other mentionable tilt-wing configurations [8–10].

Despite these efforts, controlling these aircraft, particularly during the transition phase, presents a considerable challenge due to the variations in flight dynamics. Transformational VTOL configurations, such as tilt-wings or tilt-rotors, dynamically alter their systemic form with their flight modes, resulting in a tilt of the thrust direction. From a system dynamics perspective, this results in a structural alteration of the system, which may subsequently influence the relative degree, e.g., of vertical velocity [11, 12]. These characteristics, in combination with complex aerodynamic effects and interactions, create a distinctive control problem, making the flight control law design a challenging task. This study focuses on tandem tilt-wing aircraft as one category of transformational VTOLs. However, most arguments and principles presented can be readily applied to the broader transformational VTOL category.

Common requirements for the flight control laws are its *closeness* in the sense that there are neither (explicit) switching nor predefined maneuvers involved between different flight modes, an intuitive and clean interface to the pilot that allows easy flying in the whole envelope, and an efficient use of all available control effectors [11, 12]. Widespread methods for controlling these vehicles are among multiple others [13], especially gain-scheduling of PID control laws [14], robust H_∞ control laws [15], or optimal LQR control laws [16–18], as well as adaptive control approaches [19], and dynamic inversion-based control laws [12, 20–25]. The latter is the most popular method currently

*Research Associate, Department of Aircraft Systems Dynamics, daniel.milz@dlr.de, AIAA member
†Research Associate, Department of Aircraft Systems Dynamics, marc.may@dlr.de
‡Head of Department, Department of Aircraft Systems Dynamics, gertjan.looye@dlr.de

applied. It provides an inherent solution to the aforementioned requirements while simultaneously providing physical interpretation, (global) decoupling of the dynamics, and a modular and reusable flight controller design [23].

Raab et al. propose a unified control law design approach for transformational VTOLs [12]. They specifically address the problem of changing system dynamics, particularly the relative degrees, and cope with it by distributing the control allocation to virtual control inputs, which are fed back to the reference model. Panish et al. and other research groups use nonlinear dynamic inversion (NDI) control for a (tandem) tilt-wing UAV [11, 21]. They follow a common approach in flight control design by using cascaded control loops supported by the time-scale separation principle: The controller is divided into a moment-centered rotational control loop featuring an attitude controller and control allocation strategies, wrapped by a translational control loop that tracks the flight path. However, for transformational VTOLs, the latter is generally equipped with a direct link to the primarily force-generating control effectors, which include the thrust and tilt-angle. However, this design choice already restricts certain freedoms of using the control effectors: For overactuated systems like (most) transformational VTOLs, there are multiple ways of allocating the effectors to achieve a particular effect. For instance, a tilt-wing aircraft can either change its flight path angle during cruise flight by tilting its wings and creating an upward thrust force or by changing its pitch angle.

Dynamic inversion has been shown to be a powerful control method for handling nonlinearities and decoupling nonlinear dynamics based on the physical relations of the control inputs. However, NDI demands precise knowledge of the flight dynamics - the on-board model - and estimations of the current state vector. Both pose challenges for transformational VTOLs due to their complex aerodynamic and propulsive interactions. To overcome this requirement, incremental NDI [26, 27] can be applied, canceling out internal dynamics through the time scale separation principle. While incremental NDI has several advantages over NDI, it transforms the control law into an incremental form, necessitating synchronization of signals and control actuators [28], as well as allocation of incremental commands [29]. An alternative approach [30, 31], sensory NDI, leverages the same sensor-based estimation without having incremental commands, offering a viable solution for tandem tilt-wing and transformational VTOL control. It further readily accompanies control allocation methods, which are required for such overactuated systems.

This work builds on the results and ideas of previous publications [31, 32]. [31] presents a proof-of-concept control design of a unified control law for tandem tilt-wing eVTOLs using sensory NDI and inverting the rotational and translational dynamics collectively. In [32], a generic inversion concept for transformational eVTOLs was proposed, which consists of a combined rotational and translational inversion acceleration combined with an optimization-based control allocation scheme. This study applies a previously proposed control concept for the inversion of rotational rates and velocities, and integrates it with parallel attitude and flight path control loops. These loops are designed and implemented within the scope of this work. Figure 1 shows the examined tandem tilt-wing configuration, as described in [33].

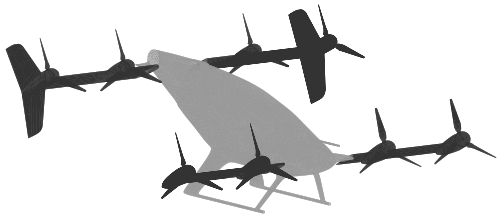

Fig. 1 Sketch of the tandem tilt-wing configuration.

This study is structured as follows: Section II details the proposed flight control law concept. Section III applies this concept to the flight control law design of a tandem tilt-wing model from [33] and implements the attitude and flight path control loops. The results of the experiments are shown in Section IV and discussed in Section V. Finally, Section VI concludes the study and gives an outlook for future work.

II. Flight Control Design

Let $x \in \mathbb{R}^{n_x}$ denote the system's state vector, $u \in \mathcal{U} \subset \mathbb{R}^{n_u}$ the input vector, and $y \in \mathbb{R}^{n_y}$ the output vector. Furthermore, let $f : \mathbb{R}^{n_x} \mapsto \mathbb{R}^{n_x}$, $g : \mathbb{R}^{n_x} \times \mathbb{R}^{n_u} \mapsto \mathbb{R}^{n_x}$, and $h : \mathbb{R}^{n_x} \times \mathbb{R}^{n_u} \mapsto \mathbb{R}^{n_x}$ be smooth vector fields. Then, a non-affine nonlinear system can be described by

$$\dot{x} = f(x) + g(x, u) \tag{1a}$$

$$y = h(x, u) \tag{1b}$$

Although most fixed-wing aircraft and the common derivation for NDI-based control laws are based on a control-affine nonlinear system, transformational VTOLs and particularly tilt-wings are inherently non-affine systems. Based on this, we will derive the nonlinear 6-DoF state space representation of the tandem tilt-wing aircraft, as shown in [33]. Let the state vector x be represented by the aircraft position in the earth frame $\boldsymbol{r}^N$, the Euler angle attitude $\boldsymbol{\theta}$, the aircraft velocity in body frame $\boldsymbol{v}^B$, and the angular rates in the body frame $\boldsymbol{\omega}^B$. Furthermore, transformational VTOLs are also described by their current *form*, which will be represented by the transformation state $\boldsymbol{\sigma}$. For instance, the current tilt angle describes the transformation state for tilt-wing VTOLs. Furthermore, let $\mathbb{T}_{\mathrm{NB}}$ and $\mathbb{T}_{\Phi\mathrm{B}}$ denote the transformation matrix from the body frame to the earth frame or the Euler angle frame, respectively, $\boldsymbol{J}$ the moment of inertia, m the total mass, and $\boldsymbol{f}^B$ and $\boldsymbol{m}^B$ the respective forces and moments in body frame. The subscript x denotes that the quantity solely depends on the state, whereas u denotes that it depends on the input and optionally the state. Then, the nonlinear state-space representation of the tandem tilt-wing eVTOL can be described by

$$\dot{\boldsymbol{r}}^N = \mathbb{T}_{\mathrm{NB}}(\theta)\, \boldsymbol{v}^B \tag{2a}$$

$$\dot{\boldsymbol{\theta}} = \mathbb{T}_{\Phi\mathrm{B}}(\theta)\, \boldsymbol{\omega}^B \tag{2b}$$

$$\dot{\boldsymbol{v}}^B = \frac{1}{m}\boldsymbol{f}^B_{\mathrm{x}}(x) - \boldsymbol{\omega}^B \times \boldsymbol{v}^B + \frac{1}{m}\boldsymbol{f}^B_{\mathrm{u}}(x, u_{\mathrm{E}}) \tag{2c}$$

$$\dot{\boldsymbol{\omega}}^B = \boldsymbol{J}^{-1}\left(\boldsymbol{m}^B_{\mathrm{x}}(x) - \boldsymbol{\omega}^B \times \boldsymbol{J}\boldsymbol{\omega}^B\right) + \boldsymbol{J}^{-1}\boldsymbol{m}^B_{\mathrm{u}}(x, u_{\mathrm{E}}) \tag{2d}$$

$$\dot{\boldsymbol{\sigma}} = f_\sigma(x) + g_\sigma(x, u_\sigma) \tag{2e}$$

with the state vector $x = \left[\boldsymbol{r}^N,\ \boldsymbol{\theta},\ \boldsymbol{v}^B,\ \boldsymbol{\omega}^B,\ \boldsymbol{\sigma}\right]$ and the input vector $u = [u_{\mathrm{E}},\ u_\sigma]$ combining the *transformation input* u_σ, which is the tilt angle $\delta_{\mathrm{w},i}$ for tilt-wing aircraft, with the other effectors u_{E}. Fig. 2 shows a sketch of the tandem tilt-wing model with inputs annotated, i.e., the tilt-wing angles $\delta_{\mathrm{w},i}$, the elevons $\delta_{\mathrm{e},i}$, and the propeller thrusts T_i.

The configuration distinguishes itself from other tilt-wing or eVTOL configurations by having eight electrically driven propellers and two independent tandem tilt-wings. The wings have vertical and horizontal displacement in order to minimize possible interactions, especially propeller-propeller interactions. Furthermore, each half-wing is equipped with one control surface combining aileron and elevator functionalities, the elevon. They lie in the wetted surface area of both propellers, which leads to an additional slipstream-interaction effect. Finally, the propeller rotation directions are chosen to allow a complete moment cancellation in nominal flight and to allow yaw maneuvers during hover flight using differential thrust.

The overall control architecture is shown in Fig. 3. Noteworthy is the combination of dynamic inversion and control allocation, as well as the parallel separation of attitude and flight path controllers. This can all be achieved through (sensory) NDI. However, coordination between the attitude and flight

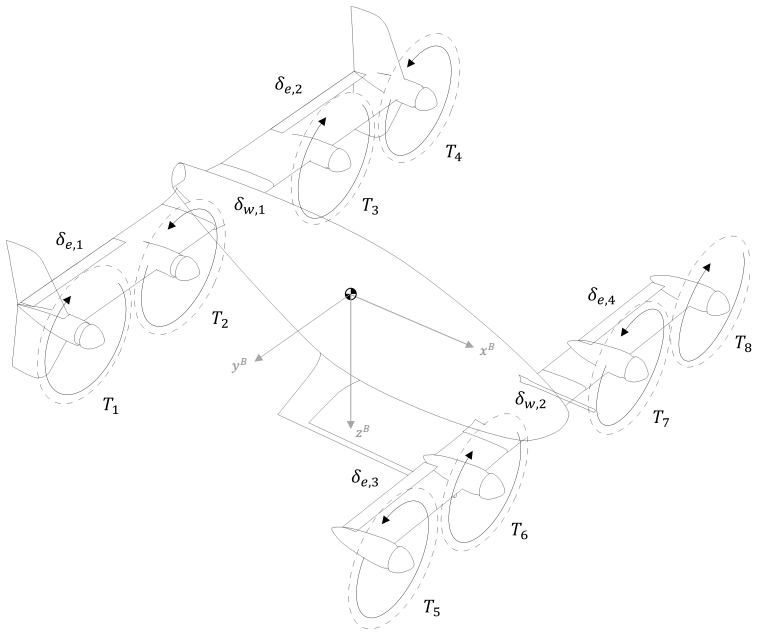

Fig. 2 3D view of the tandem tilt-wing configuration

path control loops is crucial. Furthermore, the switch between pilot inputs and autoflight functions is a handy addition for developing and researching handling qualities and pilot interactions, as well as (partly) autonomous flights.

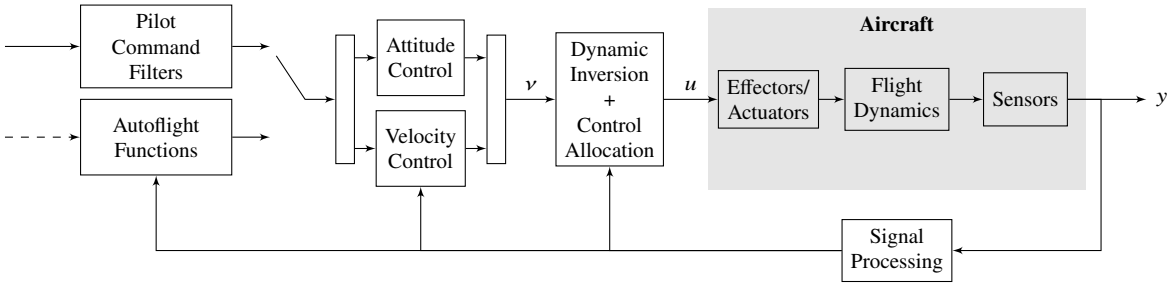

Fig. 3 Control architecture for dynamic inversion-based tandem tilt-wing control.

A. Sensory Nonlinear Dynamic Inversion

For the state-space equation (1a), the sensory NDI control law [31, 34] can be written as

$$g(\hat{x}, u) = \nu - \dot{x} + g(\hat{x}, \hat{u}) \tag{3}$$

where $\hat{}$ denotes estimated or measured quantities and $\nu \equiv \dot{y}_{\text{com}}$ the virtual control input representing the commanded state derivatives, and by applying the approximation $f(x) \approx \hat{\dot{x}} - g(\hat{x}, \hat{u})$.

The sensory NDI control design for the tandem tilt-wing eVTOL can be derived on this basis. We will invert the dynamics of $\boldsymbol{\omega}^B$, $\boldsymbol{v}_{\text{x}}^B$, and $\boldsymbol{v}_{\text{z}}^B$, which have a relative degree of 1. Note that we cannot control $\boldsymbol{v}_{\text{y}}^B$ directly in this aircraft configuration. Thus, only a subsystem of (2) is considered, consisting of (2d) and (2c). For the time being, we assume $\sigma = u_\sigma$. Finally, the sensory NDI law for the tandem tilt-wing can be stated as

$$\underbrace{\begin{bmatrix} \boldsymbol{f}_{\text{u,x}}^B(\hat{x}, u) \\ \boldsymbol{f}_{\text{u,z}}^B(\hat{x}, u) \\ | \\ \boldsymbol{m}_{\text{u}}^B(\hat{x}, u) \\ | \end{bmatrix}}_{\mathcal{F}(\hat{x}, u)} = \begin{bmatrix} m \cdot \left(\nu_{v_x} - \hat{\boldsymbol{v}}_{\text{x}}\right) + \boldsymbol{f}_{\text{u,x}}^B(\hat{x}, \hat{u}) \\ m \cdot \left(\nu_{v_z} - \hat{\boldsymbol{v}}_{\text{z}}\right) + \boldsymbol{f}_{\text{u,z}}^B(\hat{x}, \hat{u}) \\ | \\ \boldsymbol{J} \cdot \left(\nu_{\omega} - \hat{\boldsymbol{\omega}}\right) + \boldsymbol{m}_{\text{u}}^B(\hat{x}, \hat{u}) \\ | \end{bmatrix} \tag{4}$$

Note that in this formulation, the control command u is defined implicitly. Thus, we need to solve for u. The implicit function theorem or constant rank theorem states requirements for the solvability of $\mathcal{F}$ in a neighborhood of a given u_0. The implicit equation can be solved if, roughly speaking, a full-rank submatrix of the (non-square) Jacobian

$$\nabla_u \mathcal{F}(\hat{x}, u)|_{u=u_0} = \begin{bmatrix} \nabla_u \boldsymbol{f}_{\text{u,x}}^B(\hat{x}, u) \\ \nabla_u \boldsymbol{f}_{\text{u,z}}^B(\hat{x}, u) \\ \nabla_u \boldsymbol{m}_{\text{u}}^B(\hat{x}, u) \end{bmatrix}_{u=u_0} \tag{5}$$

is invertible.

B. Control Allocation and Dynamic Inversion

A detailed discussion about the design of an optimization-based control allocation in combination with dynamic inversion for transformational eVTOLs is given in [21, 32] and for other configurations in [35, 36]. Subsequently, a brief introduction is given. Solving the aforementioned dynamic inversion tracking constraint (4) requires solving the implicit equation

$$\mathcal{F}(\hat{x}, u) = \tau_0 \tag{6}$$

for $u \in \mathcal{U}$. Nevertheless, it is not possible to solve this equation explicitly for the aforementioned tandem tilt-wing configuration, given that $5 = \dim \tau_0 \lneq \dim u \geq 12$. A control allocation strategy needs to be developed in order to solve

the tracking constraint. Therefore, we will reformulate the sensory NDI law as a convex minimization problem with a linear constraint, yielding

$$\min_{u\in\mathcal{U}} L(\hat{x},u) \quad \text{s.t. } \mathcal{F}(\hat{x},u)=\tau_0 \tag{7}$$

for an arbitrary scalar cost function $L(x,u)$. In order to arrive at an explicit solution to the above problem, we utilize the Taylor series expansion in u around an arbitrary $u_0 \in \mathcal{U}$ as

$$L(x,u) = L(x,u_0) + \nabla_u L(x,u_0)(u-u_0) + \frac{1}{2}(u-u_0)^T \nabla_{uu} L(x,u_0)\,(u-u_0) + O\left((u-u_0)^3\right) \tag{8}$$

$$\mathcal{F}(x,u) = \mathcal{F}(x,u_0) + \nabla_u \mathcal{F}(x,u_0)\,(u-u_0) + O\left((u-u_0)^2\right) \tag{9}$$

Assuming sufficiently small residuals, i.e., $O\left((u-u_0)^3\right) \approx 0$ and $O\left((u-u_0)^2\right) \approx 0$, we arrive at the surrogate problem of (7):

$$\min_{u\in\mathcal{U}} \ \nabla_u L(\hat{x},u_0)\,(u-u_0) + \frac{1}{2}(u-u_0)^T \nabla_{uu} L(\hat{x},u_0)\,(u-u_0) \tag{10}$$

$$\text{s.t. } \underbrace{\nabla_u \mathcal{F}(\hat{x},u_0)}_{B}\, u = \underbrace{\tau_0 - \mathcal{F}(\hat{x},u_0) + \nabla_u \mathcal{F}(\hat{x},u_0) u_0}_{\tau} \tag{11}$$

which can be solved explicitly as [32]

$$u = B^+\tau + \left(I - B^+B\right)\left(u_0 - \nabla_{uu} L(\hat{x},u_0)^{-1}\nabla_u L(\hat{x},u_0)\right) \tag{12}$$

with the pseudo-inverse $B^+ = \nabla_{uu} L(\hat{x},u_0)^{-1} B^T \left(B\,\nabla_{uu} L(\hat{x},u_0)^{-1} B^T\right)$. This allows for an optimal control allocation fulfilling the sensory NDI tracking requirement. The latter part of (12) is a term that lies in the null space of B and thus allows a change of u without affecting the effect Bu. This can be proven through the identity $B\ (I - B^+B) = 0$.

III. Application to a Tandem Tilt-Wing eVTOL

The proposed control approach is generic for (many) transformational VTOLs. However, the application of this study is on the aforementioned tandem tilt-wing configuration (see Fig. 1). This section introduces the flight dynamic model, shows the application of the control approach to the model, and analyzes it. The model is introduced in [33] and uses a detailed strip-theory model with empirical corrections and contains a variable weight and balance model and detailed motor and propeller models. However, a simpler model is used for control design and implementation, allowing an efficient computation of the flight dynamics and quick estimation of the current B-matrix online.

A. Flight Dynamics Model

The flight dynamics model of the tandem tilt-wing aircraft (Fig. 1) is taken from a previous study [33]. It is governed by the nonlinear 6-DoF equations (2). The configuration is characterized by 14 control inputs, including eight propeller thrust commands T_i, two tilt angle commands $\delta_{\mathrm{w},i}$, and four (one per half-wing) elevon deflection commands $\delta_{\mathrm{e},i}$, as shown in Fig. 2. They allow direct control over $\boldsymbol{m}_{\mathrm{u}}^B$, and the x- and z-component of $\boldsymbol{f}_{\mathrm{u}}^B$.

The reduced model uses the same nonlinear 6-DoF equations of motion but covers the aerodynamic effects with a simplified strip-theory model following the formulation in [2, 33]. Each half wing is only divided into three *strips*: The first strip is located mainly in the slipstream of the inner half of the inner propeller, the second one in the slipstream of the outer half of the inner propeller, and the last is primarily in the slipstream of the inner half of the outer propeller. A more detailed description of this reduced strip-theory model can be found in [4]. This approach effectively accounts for the dominant effects of the tilt-wing dynamics, mainly the nonlinear and distributed aerodynamics, including propeller-slipstream effects. However, effects such as (smooth) lift distribution, propeller swirl, or interactions between the tandem wings are neglected. Yet, the quick comparison between both models shown in [4, 32] suggests that the longitudinal forces and moments match sufficiently.

B. Flight Control Law Design

The general flight control law is shown and derived in Section II, and the overall architecture is shown in Fig. 3. However, some additional discussions have to be carried out for the application of the tandem tilt-wing.

Probably the main one is the selection of controlled variables [37]. In (4), we use the body frame for the rotational and translational equations. Using ω^B seems to be a reasonable choice, especially since there exists a direct (physical) relation to the applied control effectors, and the attitude represented by Euler angles can then be controlled by using a simple kinematic relation between the angular rates and the Euler angle rates. However, the choice is not clear for the translational dynamics since those can be controlled directly through the tilt angle and thrust or indirectly through virtual control inputs in the pitch axis [12]. Thus, $\boldsymbol{v}^B$ might not be the most intuitive approach, as it suggests that both axes can be controlled independently, but actually follow the relation

$$\dot{\boldsymbol{v}}^B \sim \frac{1}{m} \cdot \sum_{i,j} \begin{bmatrix} \cos \delta_{\mathrm{w},i} \\ 0 \\ -\sin \delta_{\mathrm{w},i} \end{bmatrix} T_j \tag{13}$$

Motivated by the sinusoid relation, we will use the kinematic frame, i.e., the flight path velocity V^K and angle γ^K, in this study. [32] suggests that the flight path velocity can be controlled in the short term via the thrust and in the long term via the tilt angle, and vice versa for the flight path angle. Thus, when commanding the flight path acceleration ν_{V^K} and the flight path angle rate ν_γ, an inherent synchronization of the commanded quantities and the control inputs is established. This way, the reference models can be tuned to fit the bandwidth of the tilt-angle and thrust dynamics.

We can use the model from [33], which formulates the translation equations of motion in the body frame, by adding a kinematic transformation between the frames to convert the virtual control commands in flight path axes, ν_{V^K}, ν_γ, and ν_χ, into body axes virtual control command $\nu_{v_x^B}$, $\nu_{v_y^B}$, and $\nu_{v_z^B}$. Note that the course angle χ^K cannot be controlled directly but only indirectly via the yaw rate r during hover or the bank angle ϕ, via the roll rate p, in cruise flight. This can either by solved by using virtual control inputs as shown in [12] or by setting ν_χ to its current value, and controlling the course through a cascading control loop around the roll channel. Additionally, the side force, load factor, or acceleration can be controlled via the sideslip angle β or the yaw rate r, which is superposed with the existing feedback.

C. Flight Control Law Implementation

The flight control laws are implemented following Sections II and III.B. The cost function for the allocation is defined as the convex function

$$L(\boldsymbol{x}, \boldsymbol{u}) = \frac{1}{2} \left(\boldsymbol{u} - \boldsymbol{u}^*\right)^T \boldsymbol{W} \left(\boldsymbol{u} - \boldsymbol{u}^*\right) \tag{14}$$

with the weight matrix $\boldsymbol{W}$ chosen according to common practice as the inverse of the maximum rates of the normalized input, as

$$W_{ii} = \frac{1}{\bar{\dot{u}}_i - \underline{\dot{u}}_i} \frac{1}{\left(\bar{u}_i - \underline{u}_i\right)^2}, \qquad W_{ij} = 0 \;\; \forall\, i \neq j$$

with upper bound $\bar{u}$ and lower bound $\underline{u}$ and for the control input vector $\boldsymbol{u} = \left[n_1, \ \ldots, \ n_8, \ \delta_{\mathrm{w},1}, \ \delta_{\mathrm{w},2}, \ \delta_{\mathrm{e},1}, \ \ldots, \ \delta_{\mathrm{e},4}\right]^T$. The *optimal control input* $\boldsymbol{u}^*$ is constant throughout each time step and represents an estimated optimal allocation for the subsequent time step. In this work, $\boldsymbol{u}^*$ is set to be the current allocation with zero elevon deflection and both tilt angles equal to their average angles. This choice is intended to guide the allocation towards smooth commands, which are closely aligned with the current ones. Additionally, the total elevon deflections are reduced in order to allow for fast reactions and to avoid using them for achieving trim states. Finally, by maintaining nearly equal tilt angles, we attempt to circumvent the occurrence of uncoordinated and nonphysical allocations. This leads to the following Taylor series expansion around an arbitrary $\boldsymbol{u}_0 \in \mathcal{U}$ used the final control-allocation and inversion law (12):

$$L(\boldsymbol{x}, \boldsymbol{u}) = \underbrace{\frac{1}{2} \left(\boldsymbol{u}_0 - \boldsymbol{u}^*\right)^T \boldsymbol{W} \left(\boldsymbol{u}_0 - \boldsymbol{u}^*\right)}_{L(\boldsymbol{x}, \boldsymbol{u}_0)} + \underbrace{\left(\boldsymbol{u}_0 - \boldsymbol{u}^*\right)^T \boldsymbol{W}}_{\nabla_u L(\boldsymbol{x}, \boldsymbol{u}_0)} \left(\boldsymbol{u} - \boldsymbol{u}_0\right) + \frac{1}{2} \left(\boldsymbol{u} - \boldsymbol{u}_0\right)^T \underbrace{\boldsymbol{W}}_{\nabla_{uu} L(\boldsymbol{x}, \boldsymbol{u}_0)} \left(\boldsymbol{u} - \boldsymbol{u}_0\right) \tag{15}$$

The virtual control input vector $\boldsymbol{\nu}$ is consequently 5-dimensional and consists of rotational and translational acceleration commands, as discussed in Section III.B. The angular accelerations $\dot{\boldsymbol{\omega}}^B$ realize the Euler angle accelerations $\ddot{\phi}$, $\ddot{\theta}$, and $\ddot{\psi}$. Both quantities can be transformed analytically by means of kinematic relations. It is important to note that the following trick is applied to the yaw dynamics: the commanded $\ddot{\psi}$ for the kinematic inversion is chosen to be the current (measured) one. However, the finally propagated acceleration in body frame $\dot{r}$ is externally overwritten by either

the yaw controller in hover mode or the sideslip controller in cruise flight. The translational accelerations in horizontal and vertical directions $\dot{\boldsymbol{v}}_{\mathrm{x}}^{B}$ and $\dot{\boldsymbol{v}}_{\mathrm{z}}^{B}$ are calculated from the flight path accelerations $\dot{v}^{K}$ and $\dot{\gamma}^{K}$. Again, this transformation can be derived from kinematic relations. The virtual control input vector is thus denoted as $\boldsymbol{\nu} = \left[\nu_{\phi},\ \nu_{\theta},\ \nu_{r},\ \nu_{v^K},\ \nu_{\gamma}\right]^{T}$ where the common notation $\boldsymbol{\omega}^{B} = [p,\ q,\ r]^{T}$ is used. The virtual control input vector is calculated from a linear compensator in a PID-like structure and follows

$$\begin{bmatrix}\nu_{\phi}\\ \nu_{\theta}\end{bmatrix} = \left(\frac{K_{\mathrm{i}}}{s} + K_{\mathrm{p}}\right)\left(\begin{bmatrix}\phi_d\\ \theta_d\end{bmatrix} - \begin{bmatrix}\hat{\phi}\\ \hat{\theta}\end{bmatrix}\right) + K_{\mathrm{d}}\left(\begin{bmatrix}\dot{\phi}_d\\ \dot{\theta}_d\end{bmatrix} - \begin{bmatrix}\hat{\dot{\phi}}\\ \hat{\dot{\theta}}\end{bmatrix}\right) + K_{\mathrm{ff}}\begin{bmatrix}\ddot{\phi}_d\\ \ddot{\theta}_d\end{bmatrix} \tag{16a}$$

$$\nu_{r} = \left(\frac{K_{\mathrm{i}}}{s} + K_{\mathrm{p}}\right)(r_d - \hat{r}) \tag{16b}$$

$$\begin{bmatrix}\nu_{v^K}\\ \nu_{\gamma}\end{bmatrix} = \left(\frac{K_{\mathrm{i}}}{s} + K_{\mathrm{p}}\right)\left(\begin{bmatrix}v_d^K\\ \gamma_d\end{bmatrix} - \begin{bmatrix}\hat{v}^K\\ \hat{\gamma}\end{bmatrix}\right) \tag{16c}$$

where $_d$ denotes desired quantities and $\hat{}$ measures ones. The reference models are for both a second-order low-pass filter with a frequency of $\omega_0 = 0.5\,\mathrm{rad\,s^{-1}}$ and a damping of $\zeta = 1$. The limits for the flight path reference model are set to $\bar{V}^K = 60\,\mathrm{m\,s^{-1}}$, $\bar{\dot{V}}^K = 0.5\,\mathrm{m\,s^{-2}}$, and $\bar{\dot{\gamma}}^K = 0.05\,\mathrm{rad\,s^{-1}}$. A more detailed discussion of the control design can be found e.g., in the previous work [31] or related works [23, 38, 39].

IV. Results

The capability and accuracy of the inversion is shown and analyzed in [32]. Subsequently, the focus is on the ability to fly maneuvers and the transition. Note that in the plots, —— represent measured signals, - - - raw commands, and ····· filtered reference commands.

A. Climb maneuver with uncoupled pitch axis

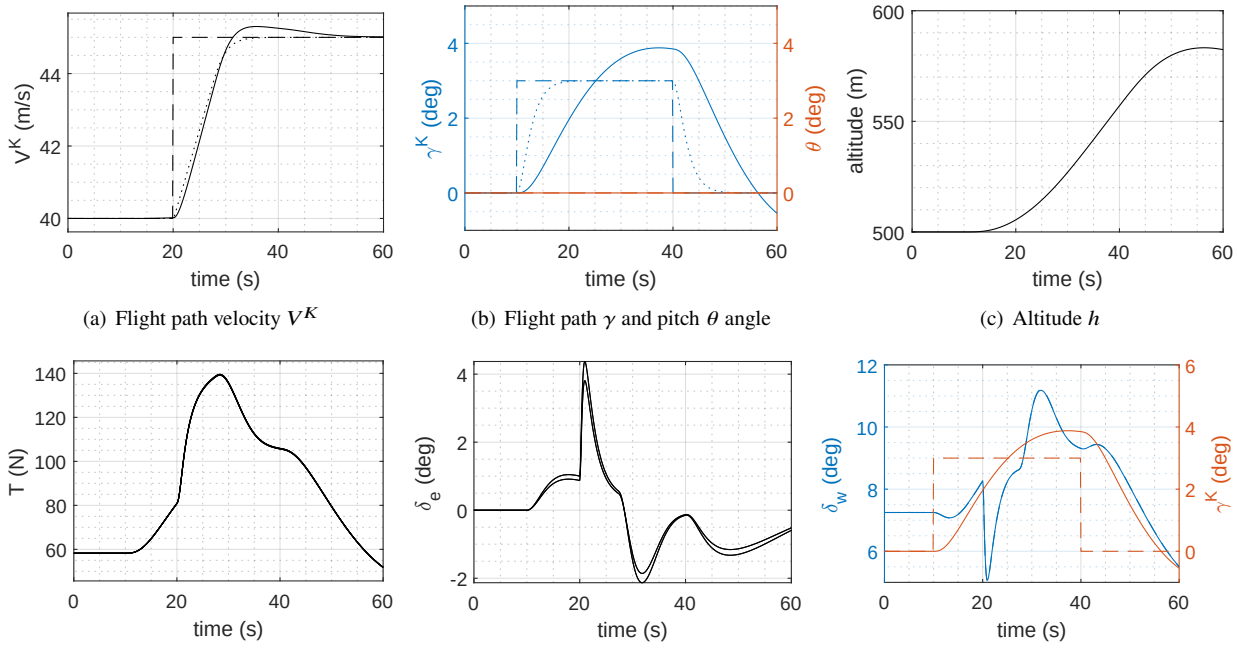

(a) Flight path velocity V^K (b) Flight path γ and pitch θ angle (c) Altitude h

(d) Thrust of each propeller T_i (e) Elevon deflections δ_e (f) Tilt δ_w and flight path γ angle

Fig. 4 Results of climb maneuver experiment with uncoupled pitch axis.

The first experiment is about decoupling the pitch axis by changing from a trimmed cruise flight state into a faster one at a higher flight level. One benefit of tilt-wing aircraft is that the flight path can be controlled independently of the

pitch axis. This can be used to allow for passenger comfort and optimal alignment of the fuselage in the airflow. In order to show this capability, the aircraft starts in trimmed cruise flight at $40\,\mathrm{m\,s^{-1}}$. At 10 s a flight path angle $\gamma = 3°$ is commanded, followed by an additional $V^K = 45\,\mathrm{m\,s^{-1}}$ command at 20 s. At 40 s, the flight path angle is set to zero again but the higher velocity is kept and a new trimmed cruise flight state is reached. The controller tracks a pitch angle of 0° throughout the whole simulation. Figure 4 shows the results of this experiment.

B. Outbound transition

The second experiment investigates the transition from hover to cruise flight. A detailed analysis of transition strategies for tandem tilt-wing aircraft is shown in [4]. For tilt-wing aircraft it is highly advisable to fly the transition in such a way that the wing (segments) do not stall. This motivates the outbound transition as a suitable maneuver as it roughly aligns the wings with the airflow (see [4]).

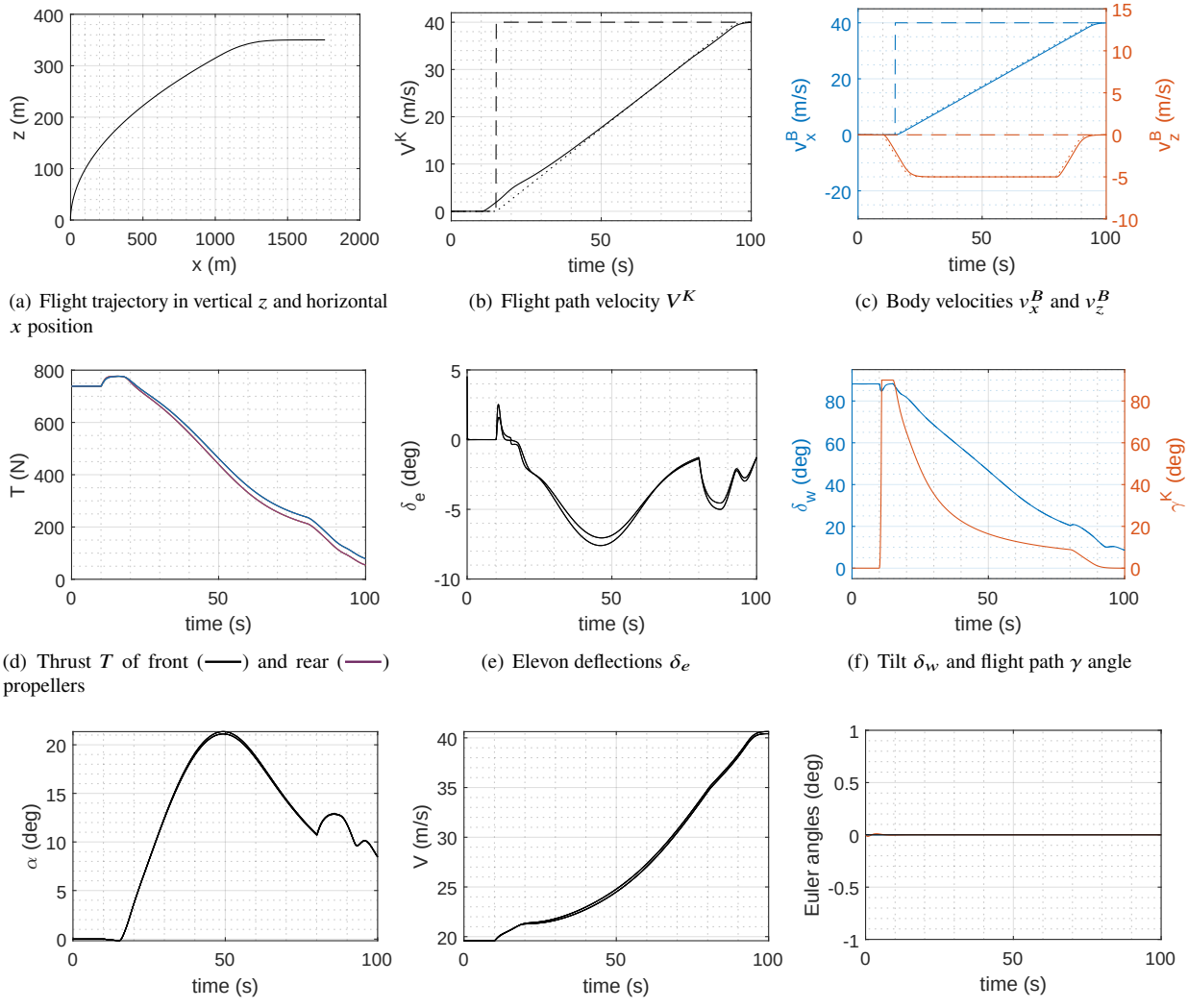

(a) Flight trajectory in vertical z and horizontal x position

(b) Flight path velocity V^K

(c) Body velocities v_x^B and v_z^B

(d) Thrust T of front (——) and rear (——) propellers

(e) Elevon deflections δ_e

(f) Tilt δ_w and flight path γ angle

(g) Effective angle of attack α_{eff} of each segment

(h) Effective airflow velocity V_{eff} of each segment

(i) Euler angles ϕ, θ, ψ

Fig. 5 Outbound transition maneuver.

For this experiment, the aircraft starts in a trimmed hover flight and is commanded a vertical velocity ($\gamma^K = 90°, V^K = 5\,\mathrm{m\,s^{-1}}$) at 10 s. This corresponds to a vertical velocity $v_z^B = -5\,\mathrm{m\,s^{-1}}$, which is hold until the late transition phase. At 15 s, an additional velocity in horizontal direction $v_x^B = 40\,\mathrm{m\,s^{-1}}$ is commanded. When reducing the vertical velocity to $0\,\mathrm{m\,s^{-1}}$ at $80\,\mathrm{m\,s^{-1}}$, the aircraft goes into a trimmed cruise flight. The flight trajectory then results in a

relatively smooth outbound transition curve. The results of the simulation are shown in Figure 5.

C. Level transition

The outbound transition maneuver is a common strategy to reach cruise flight with a tilt-wing aircraft. However, an alternative and more intuitive transition strategy is the leveled transition, where the aircraft should keep its current altitude and just accelerate in forward direction. However, this causes the wing to cross the stall region of most airfoils. Depending on the design and strategy, leveled transition is, however, a valid option for a (tandem) tilt-wing aircraft transition (see [4]). The setup is similar to the outbound transition, but this time the current flight level is kept.

Figure 6 shows the results of the experiment. Unfortunately, this maneuver is not possible with the current flight control law and aircraft design, as effective angle of attacks beyond the critical angle of attack are reached. Furthermore, note that the used flight dynamic model uses a simplified model of flow separation effects based on a 2D airfoil profile.

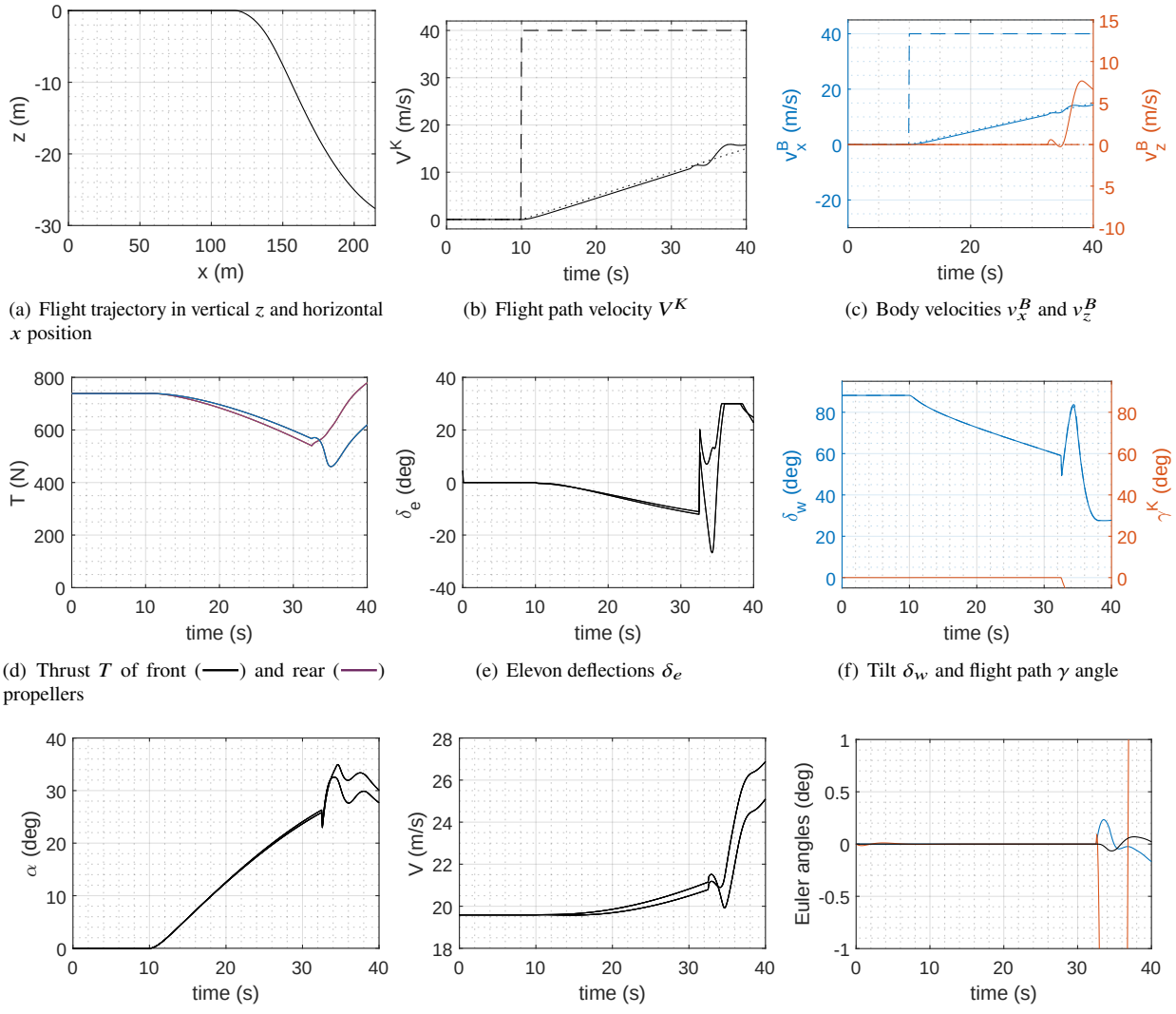

(a) Flight trajectory in vertical z and horizontal x position

(b) Flight path velocity V^K

(c) Body velocities v_x^B and v_z^B

(d) Thrust T of front (—) and rear (—) propellers

(e) Elevon deflections δ_e

(f) Tilt δ_w and flight path γ angle

(g) Effective angle of attack α_{eff} of each segment

(h) Effective airflow velocity V_{eff} of each segment

(i) Euler angles ϕ, θ, ψ

Fig. 6 Leveled transition maneuver.

V. Discussion

This paper presents the intermediate results of ongoing research on tilt-wing control strategies using dynamic inversion. It should be noted that neither the control design and implementation nor the results are final and subject to change. However, the current state is representable and should be published in order to demonstrate the approach, its capabilities, and current issues.

As the developed control concept (Section II) promises decoupling of the nonlinear dynamics, the first experiment (Section IV.A) focuses on this property in the longitudinal flight. The results demonstrate that decoupling the flight path dynamics from the pitch dynamics is possible. This opens up numerous possibilities in control design, including optimizing the control response for passenger comfort and minimizing drag. Upon closer examination of the results, it can be observed that the velocity and altitude exhibit a smooth behavior with acceptable performance. However, the flight path angle performs worse as it does not track the filtered command well. These results indicate that the proposed control law sufficiently linearizes and decouples the nonlinear coupled control channels. However, during the experiment, the aircraft remained within a limited region of the flight envelope. Consequently, the results only demonstrate a successful local inversion of the plant.

The results of the second experiment, which demonstrates the outbound transition maneuver, are presented in Section IV.B. As discussed in [4], the outbound transition is a strategy that helps to avoid flow separation during transition. Flow separation is an inherent challenge associated with tilt-wing aircraft transition maneuvers and must be considered in the control design and trajectory computation. However, there is currently no dedicated function in the controller that ensures that flow separation is avoided or a functionality that can handle flow separation within the transition. Thus, the outbound transition is a suitable starting maneuver to demonstrate the controller's capability for global inversion, excluding stall regions. The results in Section IV.B suggest, that the proposed control law can smoothly perform an outbound transition. Furthermore, it does not utilize sharp and excessive control commands but smooth ones. Moreover, flow separation is avoided, and the aircraft remains below the critical angle of attack. However, stall avoidance is achieved through the selection of the reference signal and is not yet an inherent characteristic of the control law. Nevertheless, the results indicate that the proposed control law can also invert the plant globally, in addition to the previously demonstrated local inversion capability. This can be assumed since the controller effectively decouples and tracks the velocities and attitudes throughout the maneuver, during which the aircraft crosses a large part of the flight envelope.

The final experiment, presented in Section IV.C, constitutes the subsequent step in the progression of the previous experiment. In this final experiment, an alternative transition strategy, the leveled transition, is employed. This strategy is arguably one of the most intuitive to fly but can cause flow separation on the tilt-wings. It is imperative that the final control law avoids any potentially harmful flight state. However, no protections are currently in place other than the reference model command and rate limits. The limitations of the current control implementation are revealed in the results presented in Section IV.C, where it is evident that the closed-loop aircraft is unable to perform a leveled transition. It is noteworthy that the experiment was terminated prematurely due to the emergence of unstable dynamics. Figure 6(g) shows that the effective angle of attack at the wings exceeds the stall angle, resulting in flow separation. At this point, the tilt angle has reached approximately 60°, while the forward velocity is approximately $10\,\mathrm{m\,s^{-1}}$. However, the slipstream velocity remains at approximately $20\,\mathrm{m\,s^{-1}}$, resulting in an effective angle of attack exceeding 25°, which is beyond the critical angle of attack. The results demonstrate that the proposed control law, reference model, controller gains, and command signals, as they are currently configured, cannot achieve a leveled transition. Nevertheless, the maneuver is successful up until the critical angle of attack is approached. As these are preliminary results, no countermeasures to this misbehavior have been implemented yet. However, this is part of ongoing work.

In summary, the results largely substantiate the presumed properties and capabilities of the proposed control concept. In fact, the sensory NDI law, combined with the optimization-based control allocation, can invert the tilt-wing dynamics within a safe subspace of the flight envelope, excluding post-stall regions. Consequently, this approach is a suitable candidate for further investigation. Moreover, the approach is relatively independent of the specific VTOL aircraft, suggesting potential transferability to the broader category of transformational VTOL aircraft. Nevertheless, future research must determine whether flight physical limitations, control implementation issues, or the method itself are the limiting factors for achieving a seamless inversion globally within the safe flight envelope. Therefore, a more detailed examination of the results produced by the proposed control law and the transition strategies derived from optimal control theory ([4]) will be conducted.

VI. Conclusion

Tilt-wing VTOLs, as well as transformational VTOLs, are capable of seamlessly transitioning between hover and forward flight. However, their complex mechanics, aerodynamic interactions, and changing dynamics throughout the flight phases present significant challenges for control design. In this study, a promising control approach using sensory NDI control law combined with optimization-based control allocation is implemented and tested on a tandem tilt-wing eVTOL. The angular rate and velocity inversion law is cascaded with a parallel attitude and flight path controller in order to address the multifaceted flight control task and to utilize the available degrees of freedom from the aircraft configuration. The objective is to develop a single control law that can effectively handle all flight phases of the vehicle, including the transition. The results are demonstrated using a strip theory-based 6-DoF flight dynamic model. The results substantiate the presumed properties, indicating that the control law can invert the tilt-wing dynamics within a subspace of the flight envelope, thereby allowing for the seamless execution of an outbound transition maneuver. However, when approaching flow separation on the tilt-wings, the system exhibits unstable dynamics. Therefore, future research should investigate the underlying causes of these issues, including whether they are due to physical limitations, implementation issues, or the control method. Furthermore, it is necessary to ascertain how a global inversion of the plant can be achieved. Nevertheless, this approach represents a promising candidate for further investigation, as it is potentially transferable to other transformational VTOL aircraft.

References

[1] Bacchini, A., and Cestino, E., "Electric VTOL Configurations Comparison," *Aerospace*, Vol. 6, No. 3, 2019. https://doi.org/10.3390/aerospace6030026.

[2] Cook, J., "A Strip Theory Approach to Dynamic Modeling of eVTOL Aircraft," *AIAA Scitech 2021 Forum*, 2021. https://doi.org/10.2514/6.2021-1720.

[3] Simmons, B. M., and Murphy, P. C., "Aero-Propulsive Modeling for Tilt-Wing, Distributed Propulsion Aircraft Using Wind Tunnel Data," *Journal of Aircraft*, Vol. 59, No. 5, 2022, pp. 1162–1178. https://doi.org/10.2514/1.C036351.

[4] May, M., Milz, D., and Looye, G., "Transition Strategies for Tilt-Wing Aircraft," *AIAA SciTech 2024 Forum*, 2024. https://doi.org/10.2514/6.2024-1289.

[5] Sullivan, T., "The Canadair CL-84 tilt wing design," *Aircraft Design, Systems, and Operations Meeting*, 1993. https://doi.org/10.2514/6.1993-3939.

[6] Droandi, G., Syal, M., and Bower, G., "Tiltwing Multi-Rotor Aerodynamic Modeling in Hover, Transition and Cruise Flight Conditions," *AHS International 74th Annual Forum & Technology*, 2018.

[7] North, D. D., Busan, R. C., and Howland, G., "Design and Fabrication of the LA-8 Distributed Electric Propulsion VTOL Testbed," *AIAA Scitech 2021 Forum*, 2021. https://doi.org/10.2514/6.2021-1188, URL https://arc.aiaa.org/doi/abs/10.2514/6.2021-1188.

[8] Panish, L., and Bacic, M., "Transition Trajectory Optimization for a Tiltwing VTOL Aircraft with Leading-Edge Fluid Injection Active Flow Control," *AIAA SCITECH 2022 Forum*, 2022. https://doi.org/10.2514/6.2022-1082.

[9] Holsten, J., Ostermann, T., Dobrev, Y., and Moormann, D., "Model validation of a tiltwing UAV in transition phase applying windtunnel investigations," *Congress of the International Council of the Aeronautical Sciences*, Vol. 28, International Council of the Aeronautical Sciences Bonn, Germany, 2012, pp. 1–10.

[10] Cetinsoy, E., Dikyar, S., Hancer, C., Oner, K. T., Sirimoglu, E., Unel, M., and Aksit, M. F., "Design and construction of a novel quad tilt-wing UAV," *Mechatronics*, Vol. 22, No. 6, 2012, pp. 723–745. https://doi.org/10.1016/j.mechatronics.2012.03.003.

[11] Panish, L., and Bacic, M., "A Generalized Full-Envelope Outer-Loop Feedback Linearization Control Strategy for Transition VTOL Aircraft," *AIAA AVIATION 2023 Forum*, American Institute of Aeronautics and Astronautics, 2023. https://doi.org/10.2514/6.2023-4511.

[12] Raab, S. A., Zhang, J., Bhardwaj, P., and Holzapfel, F., "Proposal of a Unified Control Strategy for Vertical Take-off and Landing Transition Aircraft Configurations," *2018 Applied Aerodynamics Conference*, American Institute of Aeronautics and Astronautics, 2018. https://doi.org/10.2514/6.2018-3478.

[13] Liu, Z., He, Y., Yang, L., and Han, J., "Control techniques of tilt rotor unmanned aerial vehicle systems: A review," *Chinese Journal of Aeronautics*, Vol. 30, No. 1, 2017, pp. 135–148. https://doi.org/10.1016/j.cja.2016.11.001.

[14] Hartmann, P., Meyer, C., and Moormann, D., "Unified Velocity Control and Flight State Transition of Unmanned Tilt-Wing Aircraft," *Journal of Guidance, Control, and Dynamics*, Vol. 40, No. 6, 2017, pp. 1348–1359. https://doi.org/10.2514/1.g002168.

[15] Dickeson, J. J., Miles, D., Cifdaloz, O., Wells, V. L., and Rodriguez, A. A., "Robust LPV H_∞ gain-scheduled hover-to-cruise conversion for a tilt-wing rotorcraft in the presence of CG variations," *2007 46th IEEE Conference on Decision and Control*, IEEE, 2007. https://doi.org/10.1109/cdc.2007.4435028.

[16] Cook, J., and Gregory, I., "A Robust Uniform Control Approach for VTOL Aircraft," *Vertical Flight Society – 2021 Autonomous VTOL Technical Meeting and Electric VTOL Symposium*, 2021.

[17] Daud Filho, A., and Belo, E., "A tilt-wing VTOL UAV configuration: Flight dynamics modelling and transition control simulation," *The Aeronautical Journal*, Vol. 128, No. 1319, 2023, pp. 152–177. https://doi.org/10.1017/aer.2023.34.

[18] Sobiesiak, L. A., Fortier-Topping, H., Beaudette, D., Bolduc-Teasdale, F., Lafontaine, J. D., Nagaty, A., Neveu, D., and Rancourt, D., "Modelling and Control of Transition Flight of an eVTOL Tandem Tilt-Wing Aircraft," *8th European Conference for Aeronautics and Aerospace Sciences (EUCASS)*, Proceedings of the 8th European Conference for Aeronautics and Space Sciences. Madrid, Spain, 1-4 july 2019, 2019. https://doi.org/10.13009/EUCASS2019-137.

[19] Axten, R. M., Khamvilai, T., and Johnson, E. N., "VTOL Freewing Design and Adaptive Controller Development," *AIAA SCITECH 2023 Forum*, 2023. https://doi.org/10.2514/6.2023-0401.

[20] Surmann, D., and Myschik, S., "Gain Design of an INDI-based Controller for a Conceptual eVTOL in a Nonlinear Simulation Environment," *AIAA SCITECH 2023 Forum*, 2023. https://doi.org/10.2514/6.2023-1250.

[21] Panish, L., Nicholls, C., and Bacic, M., "Nonlinear Dynamic Inversion Flight Control of a Tiltwing VTOL Aircraft," *AIAA SCITECH 2023 Forum*, American Institute of Aeronautics and Astronautics, 2023. https://doi.org/10.2514/6.2023-1910.

[22] Di Francesco, G., and Mattei, M., "Modeling and Incremental Nonlinear Dynamic Inversion Control of a Novel Unmanned Tiltrotor," *Journal of Aircraft*, Vol. 53, No. 1, 2016, pp. 73–86. https://doi.org/10.2514/1.C033183.

[23] Lombaerts, T., Kaneshige, J., Schuet, S., Aponso, B. L., Shish, K. H., and Hardy, G., "Dynamic Inversion based Full Envelope Flight Control for an eVTOL Vehicle using a Unified Framework," *AIAA Scitech 2020 Forum*, 2020. https://doi.org/10.2514/6.2020-1619.

[24] Binz, F., Islam, T., and Moormann, D., "Attitude control of tiltwing aircraft using a wing-fixed coordinate system and incremental nonlinear dynamic inversion," *International Journal of Micro Air Vehicles*, Vol. 11, 2019, p. 175682931986137. https://doi.org/10.1177/1756829319861370.

[25] Liu, Z., Guo, J., Li, M., Tang, S., and Wang, X., "VTOL UAV Transition Maneuver Using Incremental Nonlinear Dynamic Inversion," *International Journal of Aerospace Engineering*, Vol. 2018, 2018, pp. 1–19. https://doi.org/10.1155/2018/6315856.

[26] Chen, H. B., and Zhang, S. G., "Robust dynamic inversion flight control law design," *2008 2nd International Symposium on Systems and Control in Aerospace and Astronautics*, IEEE, 2008. https://doi.org/10.1109/isscaa.2008.4776382.

[27] Sieberling, S., Chu, Q. P., and Mulder, J. A., "Robust Flight Control Using Incremental Nonlinear Dynamic Inversion and Angular Acceleration Prediction," *Journal of Guidance, Control, and Dynamics*, Vol. 33, No. 6, 2010, pp. 1732–1742. https://doi.org/10.2514/1.49978.

[28] Kumtepe, Y., Pollack, T., and Kampen, E.-J. V., "Flight Control Law Design using Hybrid Incremental Nonlinear Dynamic Inversion," *AIAA SCITECH 2022 Forum*, American Institute of Aeronautics and Astronautics, 2022. https://doi.org/10.2514/6.2022-1597.

[29] Steffensen, R., Steinert, A., and Smeur, E. J. J., "Non-Linear Dynamic Inversion with Actuator Dynamics: an Incremental Control Perspective," *Journal of Guidance, Control, and Dynamics*, Vol. 46, No. 4, 2023, pp. 709–717. https://doi.org/10.2514/1.G007079.

[30] Smith, P., "A simplified approach to nonlinear dynamic inversion based flight control," *23rd Atmospheric Flight Mechanics Conference*, American Institute of Aeronautics and Astronautics, 1998. https://doi.org/10.2514/6.1998-4461.

[31] Milz, D., and Looye, G., "Tilt-Wing Control Design for a Unified Control Concept," *AIAA SCITECH 2022 Forum*, 2022. https://doi.org/10.2514/6.2022-1084.

[32] Milz, D., May, M., and Looye, G., "Dynamic Inversion-Based Control Concept for Transformational Tilt-Wing eVTOLs," *AIAA SciTech 2024 Forum*, AIAA, 2024. https://doi.org/10.2514/6.2024-1290.

[33] May, M. S., Milz, D., and Looye, G., "Semi-Empirical Aerodynamic Modeling Approach for Tandem Tilt-Wing eVTOL Control Design Applications," *AIAA SCITECH 2023 Forum*, 2023. https://doi.org/10.2514/6.2023-1529.

[34] Milz, D., May, M., and Looye, G., "Flight Testing Air Data Sensor Failure Handling with Hybrid Nonlinear Dynamic Inversion," *EuroGNC 2024*, 2024.

[35] Pollack, T., and Kampen, E.-J. V., "Multi-objective Design and Performance Analysis of Incremental Control Allocation-based Flight Control Laws," *AIAA SCITECH 2023 Forum*, 2023. https://doi.org/10.2514/6.2023-1249.

[36] Pfeifele, O., and Fichter, W., "Energy Optimal Control Allocation for INDI Controlled Transition Aircraft," *AIAA Scitech 2021 Forum*, 2021. https://doi.org/10.2514/6.2021-1457.

[37] Enns, D., Bugajski, D., Hendrick, R., and Stein, G., "Dynamic inversion: an evolving methodology for flight control design," *International Journal of Control*, Vol. 59, No. 1, 1994, pp. 71–91. https://doi.org/10.1080/00207179408923070.

[38] Lombaerts, T., and Looye, G., "Design and Flight Testing of Nonlinear Autoflight Control Laws," *AIAA Guidance, Navigation, and Control Conference 2012*, 2012. https://doi.org/10.2514/6.2012-4982.

[39] Grondman, F., Looye, G., Kuchar, R. O., Chu, Q. P., and Kampen, E.-J. V., "Design and Flight Testing of Incremental Nonlinear Dynamic Inversion-based Control Laws for a Passenger Aircraft," *2018 AIAA Guidance, Navigation, and Control Conference*, American Institute of Aeronautics and Astronautics, 2018. https://doi.org/10.2514/6.2018-0385.